Cellulose (2017) 24:175–190
DOI 10.1007/s10570-016-1094-8

ORIGINAL PAPER

Synthesis of core–shell structured Fe_3O_4@carboxymethyl cellulose magnetic composite for highly efficient removal of Eu(III)

Yawen Cai · Fang Yuan · Xiaomei Wang · Zhuang Sun · Yang Chen · Zhiyong Liu · Xiangke Wang · Shitong Yang · Shuao Wang

Received: 8 August 2016 / Accepted: 11 October 2016 / Published online: 19 October 2016

Abstract In this work, a carboxymethyl cellulose (CMC)-modified Fe_3O_4 (denoted as Fe_3O_4@CMC) composite was synthesized via a simple co-precipitation approach. Fourier transform infrared spectroscopy, zeta potential and thermogravimetric analysis results indicated that CMC was successfully coated on the Fe_3O_4 surfaces with a weight percent of ~30 % (w/w). The prepared Fe_3O_4@CMC composite was stable in acidic solution and could be easily collected with the aid of an external magnet. A batch technique was adopted to check the ability of the Fe_3O_4@CMC composite to remove Eu(III) as a function of various environmental parameters such as contact time, solution pH, ionic strength, solid content and temperature. The sorption kinetics process achieved equilibrium within a contact time of 7 h. The sorption isotherms were well simulated by the Langmuir model, and the maximum sorption capacity at 293 K was calculated to be 2.78×10^{-4} mol/g, being higher than the series of adsorbent materials reported to date. The ionic strength-independent sorption behaviors, desorption experiments by using ammonium acetate and disodium ethylenediamine tetraacetate as well as the spectroscopic characterization suggested that Eu(III) was sequestrated on the hydroxyl and carboxyl sites of Fe_3O_4@CMC via inner-sphere complexation. Overall, the Fe_3O_4@CMC composite could be utilized as a cost-effective adsorbent for the removal of trivalent lanthanide/actinides (e.g., $^{152+154}$Eu, ^{241}Am and ^{244}Cm) from radioactive wastewater.

Keywords Fe_3O_4@CMC · Eu(III) · Magnetic separation · Removal performance · Sorption mechanisms

Y. Cai · F. Yuan · X. Wang · Z. Sun · Y. Chen · Z. Liu · X. Wang · S. Yang (✉) · S. Wang (✉)
School for Radiological and Interdisciplinary Sciences (RAD-X), Soochow University, Suzhou 215123, People's Republic of China
e-mail: shitongyang@suda.edu.cn

S. Wang
e-mail: shuaowang@suda.edu.cn

Y. Cai · F. Yuan · X. Wang · Z. Sun · Y. Chen · Z. Liu · X. Wang · S. Yang · S. Wang
Collaborative Innovation Center of Radiation Medicine of Jiangsu Higher Education Institutions, Suzhou 215123, People's Republic of China

X. Wang
School of Environment and Chemical Engineering, North China Electric Power University, Beijing 102206, People's Republic of China

Introduction

With the rapid development of the nuclear industry and the wide operation of nuclear power plants all over the world, series of radionuclides (e.g., ^{235}U, $^{152+154}$Eu, ^{235}Np, ^{239}Pu, ^{241}Am, ^{244}Cm, etc.) are unavoidably discharged into the aquatic systems.

Exposure to the radioactive contamination can cause severe damage to the health of organisms because of its potential biological toxicity and carcinogenicity (Geckeis et al. 2013; Yang et al. 2013a; Sun et al. 2016). In view of this, it is important to develop advanced techniques that utilize environmentally friendly materials for efficient disposal of radioactive contaminants.

Sorption, as an important approach for wastewater disposal, has attracted wide attention because of its easy operation, high availability, low cost and favorable removal performance (Veliscek-Carolan et al. 2013; Sankararamakrishnan et al. 2014; Karthik and Meenakshi 2015). Recently a variety of functional materials have become available for the purification of radionuclide-bearing wastewater. For instance, fulvic acid-coated TiO_2 (denoted as TiO_2@FA) (Tan et al. 2009), cellulose acetate (CA) membrane (Zaki et al. 2012), Mg–Al layered double hydroxide intercalated with sodium lauryl sulfate (LDH-NaLS1) (Mahmoud and Someda 2012), carbon materials and their derivative composite (Fan et al. 2009a, b; Sun et al. 2012, 2013, 2016; Chang and Wu 2013; Chen et al. 2014; Xie et al. 2016) have been shown to be highly efficient for the scavenging of Eu(III) from aqueous solution. However, the difficulty of separating these adsorbents from the aqueous solution restricts their potential utilization in practical wastewater treatment. Fortunately, this problem can be resolved by introducing the magnetism of iron oxide nanoparticles for fast separation. Under the guidance of this design concept, a series of magnetic adsorbents have been synthesized and applied for the capture of Eu(III), including the cyclodextrin-decorated Fe_3O_4 composite (denoted as Fe_3O_4@CD) (Guo et al. 2015), mono-dispersed Fe_3O_4@mesoporous carbon hollow microspheres (Xu et al. 2016b), magnetite decorated graphene oxide (Li et al. 2014) and citrate-coated maghemite (Ngomsik et al. 2012). Considering their good sorption ability and excellent separation property, the magnetic composite is expected to receive ever-increasing attention in the environmental remediation field.

Carboxymethyl cellulose (CMC) is a kind of cellulose derivative with carboxymethyl (–CH_2–COOH) groups linking to some hydroxyl (–OH) sites of the glucopyranose monomers. Owing to its outstanding properties such as environmental friendliness, low cost, excellent solubility, biocompatibility and biodegradability, CMC has been extensively applied in the industrial fields of food, pharmacy, biomedicine, lithium batteries, textiles, printing, dyeing, exploration, ceramics, construction and so on (Fukami et al. 2009; Ibrahim et al. 2011; Singh and Ahmad 2012; Qiu et al. 2014). Meanwhile, CMC has been increasingly utilized as an adsorbent material in pollution control (Başarır and Bayramgil 2013; Hokkanen et al. 2014; Wang and Wang 2016). Kaur et al. (2013) proposed the strategy for high-selective separation of radionuclides by using magnetic nanoparticles conjugated with specific chelators. According to the rule of coordination chemistry, the soft metal ions preferentially bind to the soft donor atoms (e.g., S-containing functional groups), while the hard metal ions are more inclined to be coordinated by the hard donor atoms (e.g., O-donating functional groups) (Kaur et al. 2013). CMC, including abundant O-donating sites (e.g., hydroxyl and carboxyl) in its structure, is expected to exhibit unique superiority in binding trivalent lanthanides/actinides (e.g., $^{152+154}$Eu, ^{241}Am and ^{244}Cm) as hard metal ions. Herein in the present study, a CMC-decorated Fe_3O_4 magnetic material was synthesized via the chemical co-precipitation method, and the obtained Fe_3O_4@-CMC composite was applied for the decontamination of Eu(III). The physicochemical properties of this adsorbent were characterized by using powder X-ray diffraction (PXRD), Fourier transform infrared spectroscopy (FTIR), zeta potential analysis, the N_2-BET method and thermogravimetric analysis (TGA). The stability of this magnetic material in solution was evaluated by measuring the amounts of leached Fe in a wide pH range. The overall removal performance of the Fe_3O_4@CMC composite toward Eu(III) was carefully evaluated by adopting the batch technique under a series of environmental conditions. In addition, the underlying sorption mechanisms were further verified on the basis of the experimental results.

Experimental

Materials and reagents

The sodium carboxymethyl cellulose (denoted as CMC-Na) sample was purchased in analytical purity from Shanghai Yuanye Bio-Technology Co. Ltd. $Eu(NO_3)_3{\cdot}6H_2O$, $FeCl_3{\cdot}6H_2O$ and $FeCl_2{\cdot}4H_2O$ were obtained from Shanghai Energy Chemical Co., Ltd.

All other chemicals were purchased in analytical purity and directly used in the experiments. The Eu(III) stock solution was prepared by dissolving a specific amount of $Eu(NO_3)_3{\cdot}6H_2O$ in Milli-Q water.

Preparation of the Fe_3O_4 and Fe_3O_4@CMC composite

The Fe_3O_4 nanoparticles were prepared via the co-precipitation method. Typically, 9.0 g of $FeCl_3{\cdot}6H_2O$ and 3.3 g of $FeCl_2{\cdot}4H_2O$ were dissolved in 100 ml of Milli-Q water to prepare an iron-containing solution. This mixture was then added dropwise into 1.5 mol/l of NaOH solution under continuous agitation. Afterwards, the mixture was heated at 50 °C for 2 h and then cooled down to room temperature. The black precipitates were separated by an external magnet and washed repeatedly with Milli-Q water and ethanol. The wet pastes were dried overnight at 50 °C for 12 h, and then the Fe_3O_4 nanoparticles were obtained. The core–shell structured Fe_3O_4@CMC composite was synthesized through one-pot reaction. Briefly, 0.5 g of the as-prepared Fe_3O_4 sample was dispersed in 100 ml of Milli-Q water by ultrasonication; 2.5 g of CMC-Na was dissolved in 500 ml of acetic acid (5 %) solution. These two solutions were mixed, and the resulting mixture was mechanically stirred at 75 °C for 24 h. The suspension was exposed to an external magnet to separate the solid from the liquid phase. The collected wet pastes were then rinsed several times with Milli-Q water followed by ethanol. The products were dried at 50 °C overnight in a vacuum oven.

Characterization of magnetic materials

The PXRD patterns of Fe_3O_4 and the Fe_3O_4@CMC composite were collected on a Bruker D8 Advance diffractometer with Cu-Kα ($\lambda = 1.54056$ Å) radiation. FTIR spectra of magnetic materials and pure CMC-Na in the range of 4000–400 cm^{-1} were recorded on a Thermo Nicolet 6700 spectrometer. The zeta potentials of Fe_3O_4 and the Fe_3O_4@CMC composite in the pH range of 2.0–9.0 were measured with the aid of a Zetasizer Nano ZS90 Analyzer. The zero point charge (pH_{zpc}) values for these two materials were obtained by interpolating the zeta potential data to zero. The thermogravimetric curves within 30–900 °C were collected on a NETZSCH STA 449F3 instrument under a nitrogen flow. According to the N_2-BET method, the specific surface areas of Fe_3O_4 nanoparticles and the Fe_3O_4@CMC composite were measured to be 66.2 and 52.0 m^2/g, respectively. The stability of Fe_3O_4 nanoparticles and the Fe_3O_4@CMC composite were evaluated by dispersing these two magnetic samples into a series of $NaNO_3$ solutions within pH 2.0–10.0. The suspensions were gently oscillated for 24 h, and the solid and liquid phases were separated by exposure to an external magnet. The supernatants were filtered through a 0.22-μm filtration membrane, and the amounts of dissolved iron were quantitatively measured by using inductively coupled plasma-atomic emission spectrometry (ICP-AES).

Sorption experiments

The batch experiments for Eu(III) sorption on magnetic materials were performed in a series of 10-ml polyethylene centrifuge tubes. Specifically, the suspensions of sorbent materials, $NaNO_3$ electrolyte solution and Eu(III) stock solution were added to achieve their specified concentrations. The pH values were adjusted by adding inappreciable amounts of HNO_3 and/or NaOH solutions. The centrifuge tubes were gently oscillated for 24 h to achieve the sorption equilibrium. Afterwards, an external magnet was used to separate the solid from the aqueous phase. The supernatants were filtered with a 0.22-μm filtration membrane, and the final concentrations of Eu(III) were determined by using ICP-AES and/or inductively coupled plasma-mass spectrometry (ICP-MS). The sorption percentage (sorption $\% = (C_0 - C_e)/C_0 \times 100\ \%$), sorption amount ($q_e = (C_0 - C_e)$ V/m, mol/g) and distribution coefficient ($K_d = q_e/C_e$, L/g) were then calculated from the initial Eu(III) concentration (C_0, mol/l), residual Eu(III) concentration (C_e, mol/l) and the solid-to-liquid ratio (m/V, g/l) of magnetic materials.

Results and discussion

Characterization of magnetic materials

Figure 1a displays the PXRD patterns of the synthesized Fe_3O_4 and Fe_3O_4@CMC composite. Both of the two curves present three dominating diffraction peaks at 30.1°, 35.6° and 43.3°, which correspond to the

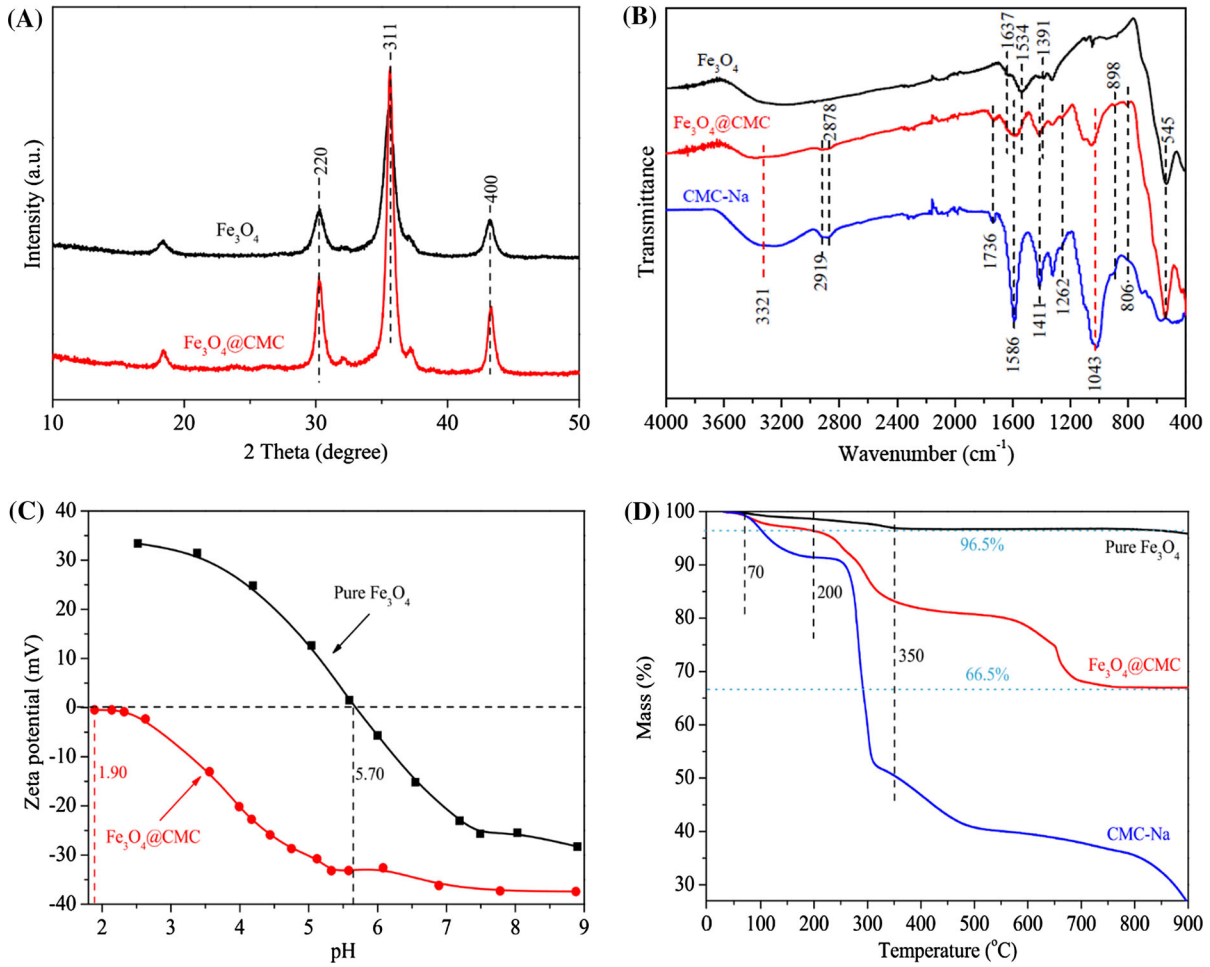

Fig. 1 **a** PXRD patterns of pure Fe_3O_4 and Fe_3O_4@CMC composite; **b** FTIR spectra of pure Fe_3O_4, CMC and Fe_3O_4@-CMC composite; **c** zeta potentials of pure Fe_3O_4 and Fe_3O_4@-CMC composite at various solution pH values. $T = 293$ K, m/V = 0.2 g/l, $I = 0.01$ mol/l $NaNO_3$; **d** thermogravimetric curves of pure Fe_3O_4, CMC and Fe_3O_4@CMC composite

characteristic (220), (311) and (400) planes of the cubic Fe_3O_4 phase (JCPDS no. 85–1436). No obvious difference can be found between the two patterns, which suggests that the surface decoration of Fe_3O_4 cores with a CMC shell does not change its crystalline structure. Figure 1b shows the FTIR spectra of Fe_3O_4 nanoparticles, CMC-Na and Fe_3O_4@CMC. For Fe_3O_4 and Fe_3O_4@CMC, the peak at 545 cm^{-1} represents the characteristic stretching vibration of the Fe–O bond (Rajput et al. 2016). It is noteworthy that the FTIR spectrum of Fe_3O_4 exhibits some additional peaks between 1200 and 1650 cm^{-1} by comparison with those reported in the previous literatures (Liu et al. 2008; Rajput et al. 2016). In the present study, the Fe_3O_4 nanoparticles were synthetized under ambient conditions. In view of this, the dissolution of CO_2 gas from the air into the reaction system could not be avoided. The dissolved CO_2 would be adsorbed on the hydroxylated Fe_3O_4 surfaces, resulting in the formation of bicarbonate and carbonate (Baltrusaitis et al. 2006). Specifically, the peaks at 1391, 1534 and 1637 cm^{-1} can be assigned to the OCO stretching vibrations of adsorbed bicarbonate/carbonate (Baltrusaitis et al. 2006). For pure CMC-Na, the broad band located at 3321 cm^{-1} is attributed to the O–H stretching vibration. The bands at 2919 and 2878 cm^{-1} belong to the stretching vibrations of $–CH_2$ and $–CH_3$ in the CMC structure, respectively. The peak at 1736 cm^{-1} is assigned to the stretching vibration of C=O bond in ester groups. The peak at

1586 cm^{-1} is due to the asymmetry stretching vibration of –COO bond in the structure of carboxylic salt, and the peak at 1411 cm^{-1} originates from the symmetry stretching vibration of –COO bond (Lin et al. 2015; Yeasmin and Mondal 2015). The band at 1262 cm^{-1} is induced by the stretching vibration of the C–O bond of the CMC carbonate sites. The peak at 1043 cm^{-1} is ascribed to the stretching vibration of the O–C–C bond (Sitthichai et al. 2015). The bands at 898 and 806 cm^{-1} are assigned to the glucosidic bond in the CMC structure. These characteristic bands are present in the FITR spectrum of the Fe_3O_4@CMC composite, suggesting that the CMC moieties have been successfully introduced on the Fe_3O_4 surfaces. Specifically, the bands at 3321 and 1043 cm^{-1} for the CMC-Na shift to 3418 and 1050 cm^{-1} for the Fe_3O_4@CMC composite, respectively. This variation trend indicates that the O–H and O–C–C bonds of CMC-Na are possibly involved in the formation of Fe_3O_4@CMC.

From the zeta potential data as shown in Fig. 1c, the pH_{zpc} value of Fe_3O_4 nanoparticles is identified to be ~5.70. It is worth noting that this value is lower than those reported in the previous studies (i.e., mostly ranging from 6.0 to 7.0) (Chang and Chen 2005; Liu et al. 2008). As indicated by the FTIR spectrum (Fig. 1b), the attachment of dissolved CO_2 on the surfaces of synthesized Fe_3O_4 nanoparticles results in the formation of bicarbonate/carbonate. These surface-adsorbed anionic components would correspondingly reduce the zeta potentials of the Fe_3O_4 sample. The pH_{zpc} value of the Fe_3O_4@CMC composite (~1.90) is much lower than that of Fe_3O_4 nanoparticles, which evidently demonstrates the successful decoration of CMC onto Fe_3O_4 surfaces. Note that the pH_{zpc} value of the Fe_3O_4@CMC composite is lower than the pK_a value of CMC (3.2–4.3) reported in the previous literatures (Zhivkov 2013; Dogsa et al. 2014; Matthew et al. 2015). This phenomenon can be tentatively interpreted by considering the synthesis condition and the CMC properties. Herein, the Fe_3O_4@CMC composite was synthesized via the surface grafting reaction under acidic conditions. In a previous study, Xu et al. (2006) synthesized an alginate-coated Fe_3O_4 composite at pH 4.0 by using a similar method. The zeta potential of the prepared composite was negative even at pH 2.5, which was lower than the reported pK_a value of alginate (3.4–4.2) (Lamelas et al. 2005; Lagoa and Rodrigues 2007; Obeid et al. 2014). The authors proposed that the surface charge of the alginate-coated Fe_3O_4 composite was dependent on the sorption amount and ionization degree of alginate. At pH 4.0, the active –FeOH groups of Fe_3O_4 nanoparticles were effectively replaced by the –COO groups of alginate, which greatly reduced the zeta potential of the synthesized composite. The molecular structure of CMC is similar to that of alginate. In view of this, the low pH_{zpc} of the Fe_3O_4@CMC composite in our present study can be partly attributed to the acidic synthesis condition. In addition, the degree of substitution (i.e., the degree of hydroxyl in the structure of the glucose ring replaced by the carboxymethyl) and molecular weight of CMC may also influence the zeta potentials of the prepared Fe_3O_4@CMC composite.

TGA can be used to quantitatively determine the relative amount of ligand grafted on the surfaces of substrate material. The TG curves of Fe_3O_4 nanoparticles, the Fe_3O_4@CMC composite and CMC-Na are shown in Fig. 1d. Specifically, the incipient gentle declines within 70–200 °C can be ascribed to the degradation of impurities and the evaporation of adsorbed water and moisture. The dominating weight loss of CMC-Na and the Fe_3O_4@CMC composite from 200 to 350 °C results from the decarboxylic reaction of CMC molecules (Sitthichai et al. 2015). The weight loss of the Fe_3O_4@CMC composite at temperatures higher than 350 °C originates from the potential rupture of the internal chemical bonds. As shown in Fig. 1d, the pure Fe_3O_4 nanoparticles show no weight loss within this temperature range. In view of this, the observed weight loss is due to the fracture of C–O bonds in the CMC structure. By considering the weight loss of Fe_3O_4@CMC from ~96.5 % at 200 °C to ~66.5 % at 900 °C, the weight percent of surface-coated CMC is calculated to be ~30 % (w/w). These CMC moieties would provide plentiful functional groups (e.g., hydroxyl –OH and carboxyl –COOH) for binding Eu(III).

Figure 2 presents the amounts of Fe leaching from pure Fe_3O_4 and the Fe_3O_4@CMC composite within the pH range of 2.0–9.0. Clearly, these two materials are relatively resistant to the acidic condition with a small amount of dissolved iron (~0.02 mmol/l) at a low pH value of 2.0. The concentration of leached Fe sharply decreases with increasing pH, and no soluble Fe can be detected at pH > 5.0. Herein, the magnetic adsorbents are synthesized via the co-precipitation

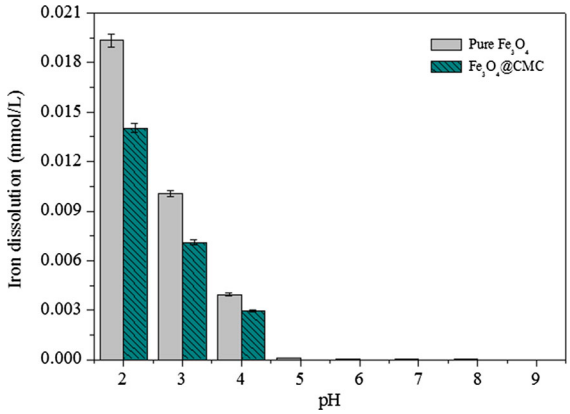

Fig. 2 Relative amount of Fe leaching from pure Fe_3O_4 and the Fe_3O_4@CMC composite at various solution pH values. $T = 293$ K, m/V = 0.2 g/l, $I = 0.01$ mol/l $NaNO_3$

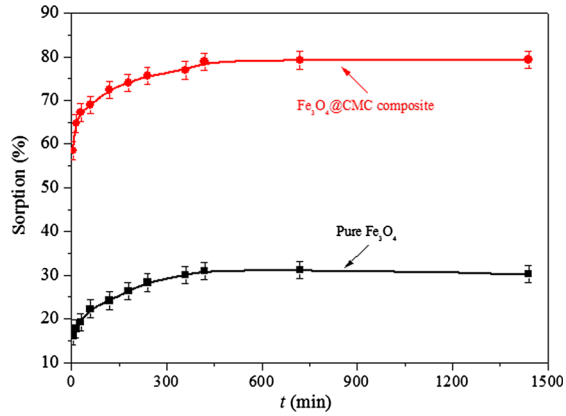

Fig. 3 Time-dependent sorption behaviors of Eu(III) on pure Fe_3O_4 and Fe_3O_4@CMC composite. $T = 293$ K, pH = 5.5, m/V = 0.2 g/l, $C_{Eu(III)initial} = 5 \times 10^{-5}$ mol/l, $I = 0.01$ mol/l $NaNO_3$

method under high alkaline conditions. In view of this, they are expected to be more stable at higher pH values. Note that the Fe-leaching degree in case of the Fe_3O_4@CMC composite is lower than that of Fe_3O_4 nanoparticles at pH 2.0–4.0, indicating that the surface coating of CMC layers effectively protects the Fe_3O_4 inner cores from dissolution and thus enhances the acidic tolerance of the as-prepared Fe_3O_4@CMC composite. By considering the requirement on the stability and durability of adsorbents, the Fe_3O_4@-CMC composite can be applied for the decontamination of environmental pollutants from various aquatic systems over a wide pH range.

Sorption kinetics

Figure 3 shows the kinetics data of Eu(III) sorption on pure Fe_3O_4 and the Fe_3O_4@CMC composite. The sorption percentage gradually increases with prolonged contact time and finally reaches equilibrium after 420 min (i.e., 7 h). The nano-scaled size of pure Fe_3O_4 particles facilitates the transport of Eu(III) species in the bulk solution onto their surfaces without perceptible resistance (Zhang et al. 2010). For Fe_3O_4@CMC composite, the carboxyl (–COOH) and hydroxyl (–OH) sites of the surface-coated CMC moieties show high complexing affinity for Eu(III) (Kaur et al. 2013). The absence of internal diffusion resistance results in a favorable sorption kinetics procedure. According to the experimental data herein, a contact time of 24 h is selected in the following experiments to ensure the achievement of sorption equilibrium.

In order to determine the controlling mechanisms during the entire sorption process, the experimental kinetics data were simulated with the pseudo-first-order (Eq. 1) and pseudo-second-order models (Eq. 2) as listed below (Yang et al. 2013a; Ho and McKay 1999a, b; Ho and Ofomaja 2006):

$$\ln(q_{e,exp} - q_t) = \ln q_{e,cal} - k_1 t \quad (1)$$

$$\frac{t}{q_t} = \frac{1}{k_2 q_{e,cal}^2} + \frac{1}{q_{e,cal}} t \quad (2)$$

herein k_1 (min^{-1}) and k_2 (g/(mol min)) refer to the rate constants of pseudo-first-order and pseudo-second-order models, respectively; q_t (mol/g) and $q_{e,exp}$ (mol/g) are the experimental sorption amounts of Eu(III) at a specific time and equilibrium time, respectively; $q_{e,cal}$ represents the theoretical sorption amount (mol/g) as predicted by the kinetics models. Figure 4a, b illustrates the intuitive fitting results by using the linear forms of pseudo-first-order and pseudo-second-order models, respectively. The corresponding kinetic parameters calculated from the model fits are listed in Table 1. According to the R^2 values, the sorption kinetic data are better simulated by the pseudo-second-order model than the pseudo-first-order model. Accordingly, the $q_{e,cal}$ values obtained from pseudo-second-order model fits are almost equivalent to the $q_{e,exp}$ values, while those calculated from the pseudo-first-order model fits are much lower than the $q_{e,exp}$

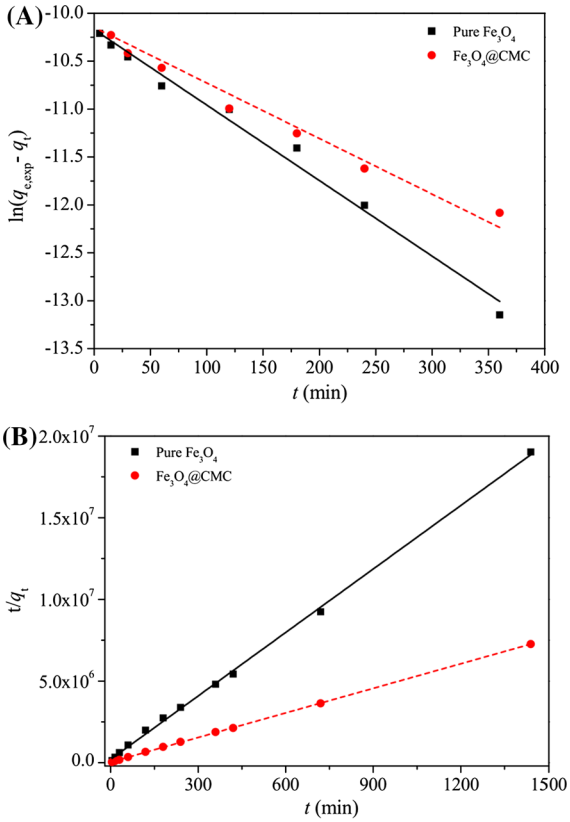

Fig. 4 The fit curves of sorption kinetics data by pseudo-first-order (**a**) and pseudo-second-order (**b**) equations. The *solid* and *dash lines* represent the model fits for Eu(III) sorption on pure Fe_3O_4 and Fe_3O_4@CMC composite, respectively

values. This phenomenon demonstrates that the rate-controlling mechanism involved in the sorption kinetics of Eu(III) is chemisorption rather than physical interactions or mass transport (Chen et al. 2009; Chiou and Li 2003). More specifically, the chemisorption of Eu(III) on magnetic materials would result in the formation of surface complexes.

Figure 3 and Table 1 show the sorption amount of Eu(III) on the Fe_3O_4@CMC composite is much higher than that on bare Fe_3O_4 nanoparticles. This phenomenon is not induced by the difference of specific surface area between the Fe_3O_4@CMC composite (66 m^2/g) and Fe_3O_4 nanoparticles (52 m^2/g). Alternatively, the higher sorption performance of the Fe_3O_4@CMC composite toward Eu(III) is expected to result from the surface-linked CMC moieties. As mentioned above, the Fe_3O_4@CMC composite possesses higher stability in solution than the Fe_3O_4 nanoparticles. In addition, the modification of Fe_3O_4 nanoparticles with CMC coating would efficiently reduce their agglomeration in the solution as proposed in previous studies (Liu et al. 2008; Yang et al. 2012), which correspondingly enhances the dispersion of the Fe_3O_4@CMC composite. As a result, the surface sites would be more available for binding Eu(III). Herein, the kinetics experiments are performed at a pH value of 5.5, which is lower than the pH_{zpc} value of Fe_3O_4 nanoparticles (5.70), while higher than that of the Fe_3O_4@CMC composite (1.90). Thereby, the Fe_3O_4 surfaces are positively charged because of the protonation reaction, while the surfaces of the Fe_3O_4@CMC composite are negatively charged because of the deprotonation reaction. Owing to the electrostatic attraction, the Eu(III) species (mainly positive Eu^{3+} ions at pH 5.5) would be preferentially retained on the Fe_3O_4@CMC surfaces, resulting in a higher sorption amount.

Effect of solution pH and ionic strength

Figure 5 shows the pH-dependent sorption trends of Eu(III) on the Fe_3O_4@CMC composite at a series of ionic strength, i.e., 0.001, 0.005 and 0.01 mol/l of $NaNO_3$ electrolyte solution. Specifically, the variation

Table 1 The kinetics parameters of Eu(III) sorption on pure Fe_3O_4 and Fe_3O_4@CMC composite

Kinetics models	Parameters	Pure Fe_3O_4	Fe_3O_4@CMC composite
Pseudo-first order	k_1 (min^{-1})	7.88×10^{-3}	5.80×10^{-3}
	$q_{e,exp}$ (mol/g)	7.70×10^{-5}	1.98×10^{-4}
	$q_{e,cal}$ (mol/g)	3.83×10^{-5}	3.92×10^{-5}
	R^2	0.970	0.891
Pseudo-second order	k_2 (g/(mol min))	819.93	616.21
	$q_{e,exp}$ (mol/g)	7.70×10^{-5}	1.98×10^{-4}
	$q_{e,cal}$ (mol/g)	7.72×10^{-5}	1.99×10^{-4}
	R^2	0.998	0.999

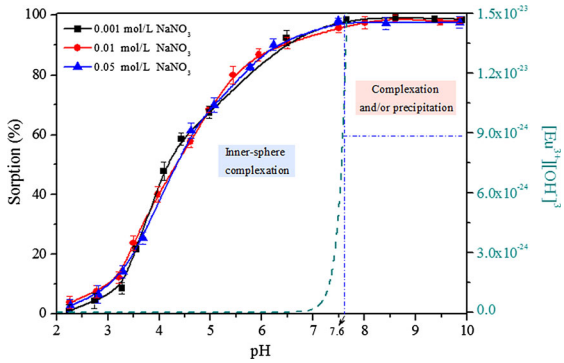

Fig. 5 Effect of pH and ionic strength on Eu(III) sorption on Fe_3O_4@CMC composite. $T = 293$ K, m/V = 0.2 g/l, $C_{(Eu(III))initial} = 5 \times 10^{-5}$ mol/l

of ionic strength has ignorable influence on Eu(III) removal within the whole pH range. The sorption data as a function of ionic strength can be used to help determine the underlying removal mechanisms. Generally, the independence of sorption trend on ionic strength suggests the occurrence of inner-sphere complexation and or precipitation (Yang et al. 2012, 2014; Tan et al. 2014), while the ionic strength-dependent sorption trend is due to ion exchange and/or outer-sphere complexation (Fan et al. 2009a, b; Chang and Wu 2013; Fukushi et al. 2013; Sheng et al. 2014). Herein, the negligible effect of ionic strength indicates that the removal of Eu(III) by Fe_3O_4@CMC is induced by inner-sphere complexation and/or precipitation.l

One can see from Fig. 5 that the sorption percentage of Eu(III) gradually increases from ~5 to ~100 % as the solution pH rises from 2.0 to 7.5 and then keeps at a high value at pH > 7.5. Herein, the sorption trend can be interpreted by considering the surface properties of the Fe_3O_4@CMC composite and the speciation of Eu(III) in solution. As mentioned above, the Fe_3O_4@CMC composite has a pH_{zpc} value of ~1.90 (Fig. 1c). In view of this, the surfaces of this material are negatively charged within the pH range of our experiments (2.0–10.0). More specifically, the surfaces would become more negatively charged at higher pH values because of the enhanced deprotonation reaction, which correspondingly strengthens the chemical interactions between the Eu(III) species and the deprotonated surface sites. It is necessary to check whether the precipitation of $Eu(OH)_3$(s) phase contributes to the removal of Eu(III). In view of this, the pH-dependent precipitation curve of Eu(III) as derived from the initial Eu(III) concentration (i.e., 5.0×10^{-5} mol/l) and the solubility product constant of $Eu(OH)_3$(s) (8.9×10^{-24}) is also illustrated in Fig. 5. Clearly, the aqueous Eu(III) species begins to form a precipitate from a pH value of 7.6. In view of this, the capture of Eu(III) by Fe_3O_4@CMC at pH < 7.6 is due to inner-sphere complexation rather than precipitation.

Effect of solid content

Solid dosage is one of the important factors that should be taken into consideration when evaluating the price-performance ratio of sorbents in wastewater treatment. In view of this, the sorption of Eu(III) on the Fe_3O_4@CMC composite as a function of solid content (g/l) was studied, and the results are illustrated in Fig. 6. Specifically, the sorption percentage gradually increases from ~65 to ~99 % as the solid content

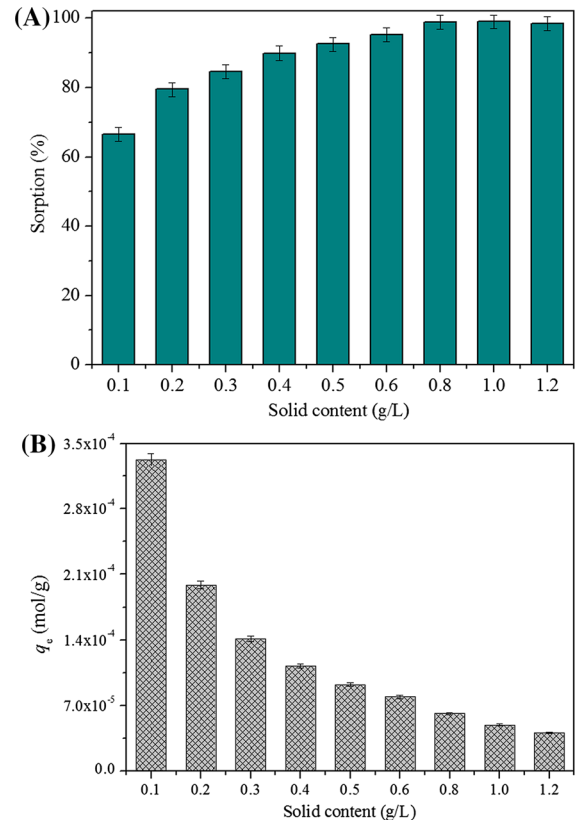

Fig. 6 Sorption percentage (**a**) and sorption amount (**b**) of Eu(III) on Fe_3O_4@CMC composite. $T = 293$ K, pH = 5.5, $C_{Eu(III)initial} = 5 \times 10^{-5}$ mol/l, $I = 0.01$ mol/l $NaNO_3$

rises from 0.1 to 0.8 g/l and then stays constant at a higher solid-to-liquid ratio (Fig. 6a). With increasing solid dosage, more active sites can be provided by the Fe_3O_4@CMC composite to form complexes with Eu(III), resulting in the increase of Eu(III) sorption percentage. It is clear that the sorption percentage of Eu(III) would not unboundedly increase with the growth of the solid dosage. In practical wastewater disposal, it is necessary to adopt a proper sorbent dosage on the basis of the initial metal ion concentration and the relevant environmental standards so as to reduce the treatment cost. According to the experimental result herein, a solid-to-liquid ratio of 0.8 g/l is the optimum dosage for the Fe_3O_4@CMC composite to decontaminate Eu(III) with an initial concentration of 5.0×10^{-5} mol/l.

As shown in Fig. 6b, the sorption amount of Eu(III) gradually decreases with increasing Fe_3O_4@CMC dosage. Herein, the significant negative correlation can be interpreted from the following aspects. At lower solid dosage, the Fe_3O_4@CMC particles exhibit good dispersity, and the surface active sites are highly available for binding Eu(III). In contrast, higher sorbent dosage would lead to the supersaturation of the suspension, which results in the collision and aggregation of Fe_3O_4@CMC particles. Consequently, the availability of the surface sites would be greatly reduced, and then the decrease of Eu(III) sorption amount is expected under such circumstances. In addition, the inter-collision between Fe_3O_4@CMC particles at higher solid content may lead to the release of some surface-linked Eu(III) species back into the solution. Moreover, the aggregation of solid particles may decrease the total surface area of the Fe_3O_4@-CMC composite and prolong the diffusional path for the close attachment of Eu(III) on its surface sites (Shukla et al. 2002). These variation trends would collectively cause the decrease of Eu(III) sorption amount.

Sorption isotherms and thermodynamic data

Figure 7 illustrates the sorption isotherms of Eu(III) on the Fe_3O_4@CMC composite at three different temperatures, viz., 293, 313 and 333 K. Clearly, the sorption curves exhibit the conventional L type with a visible platform for the Eu(III) sorption amount, ruling out the potential occurrence of precipitation during the removal procedure. It is clear that the sorption amount

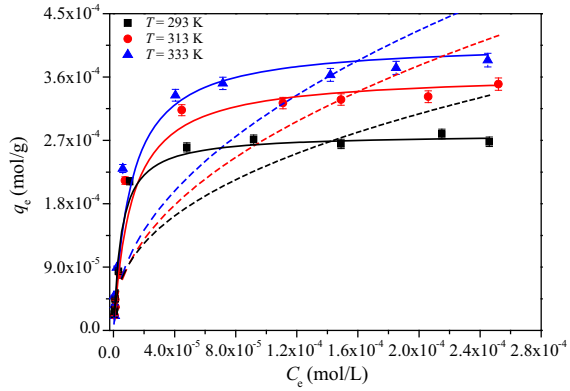

Fig. 7 Sorption isotherms, Langmuir and Freundlich model fits of Eu(III) on Fe_3O_4@CMC composite. pH = 5.5, m/V = 0.2 g/l, I = 0.01 mol/l $NaNO_3$. *Symbols* represent the experimental data, the *solid lines* represent the fit curves of the Langmuir model, and the *dash lines* represent the fit curves of the Freundlich model

of Eu(III) is the lowest at 293 K and is the highest at 333 K, which suggests that the increase of temperature is beneficial for Eu(III) removal. To help deduce the underlying removal mechanisms, the sorption isotherms were simulated by using the Langmuir and Freundlich models as described below (Bulut et al. 2008):

$$\text{Langmuir:} \quad q_e = \frac{bq_{max}C_e}{1 + bC_e} \tag{3}$$

$$\text{Freundlich:} \quad q_e = K_F C_e^n \tag{4}$$

herein C_e (mol/l) is the residual Eu(III) concentration after sorption equilibrium, q_e (mol/g) is the equilibrium Eu(III) sorption amount on per weight unit of the Fe_3O_4@CMC composite, and q_{max} (mol/g) is the maximum sorption capacity of the Fe_3O_4@CMC composite toward Eu(III) under a condition of monolayer coverage. b, K_F and n are sorption indexes that are related to the temperature.

The parameters derived from the model fit are listed in Table 2. According to the correlation coefficient (R^2) values, the sorption isotherm data are better fitted by the Langmuir model. This phenomenon suggests that the sequestration of Eu(III) on the Fe_3O_4@CMC composite is a chemical sorption process (Zhou et al. 2009; Yang et al. 2010, 2015). Note that the sorption isotherm experiments were carried out at a constant Fe_3O_4@CMC content of 0.2 g/l. This means that a finite amount of surface sites would be provided for

Table 2 Parameters for Langmuir and Freundlich models at different temperatures

Correlation parameters	$T = 293$ K	$T = 313$ K	$T = 333$ K
Langmuir			
q_{max} (mol/g)	2.78×10^{-4}	3.57×10^{-4}	3.91×10^{-4}
b (l/mol)	2.08×10^{5}	1.29×10^{5}	9.60×10^{4}
R^2	0.988	0.974	0.982
Freundlich			
K_F (mol^{1-n} L^n/g)	2.12×10^{-3}	3.48×10^{-3}	3.93×10^{-3}
n	0.291	0.262	0.235
R^2	0.844	0.863	0.861

binding Eu(III), leading to the appearance of a saturated sorption amount at higher Eu(III) concentration. Under such circumstances, the sorption isotherms would not be well simulated by the Freundlich model with the assumption of an exponential increase of the Eu(III) sorption amount with increasing Eu(III) concentration. At the three temperatures, the experimental q_e values are smaller than the q_{max} values as obtained from the Langmuir model fits. This phenomenon indicates that the surfaces of Fe_3O_4@CMC are not fully saturated and Eu(III) is adsorbed in a monolayer mode. The n values are calculated to be smaller than 1, indicating the occurrence of a nonlinear sorption process.

To further determine the effect of temperature on the sorption behaviors of Eu(III), the following equations were used to calculate the intrinsic thermodynamic parameters involved in the sorption process, including the changes of Gibbs free energy (ΔG^0), enthalpy (ΔH^0) and entropy (ΔS^0).

$$\Delta G^0 = -RT \ln K^0 \tag{5}$$

$$\Delta S^0 = -\left(\frac{\partial \Delta G^0}{\partial T}\right)_P \tag{6}$$

$$\Delta H^0 = \Delta G^0 + T\Delta S^0 \tag{7}$$

herein K^0 (l/g) is the sorption equilibrium constant. The values of $\ln K^0$ can be obtained from the linear plot of $\ln K_d$ versus q_e. The calculated thermodynamic data from the foregoing equations are listed in Table 3. The positive ΔH^0 values suggest that the removal of Eu(III) by the Fe_3O_4@CMC composite is an endothermic process. This result can be interpreted from the following aspects: (1) higher temperature is conducive to the diffusion, migration and attachment of Eu(III) from the aqueous solution onto the Fe_3O_4@CMC surfaces; (2) the loss of coordinated water molecules in the hydration shell of Eu(III) is the precondition for the surface complexation. This dehydration process is endothermic and is more favored at higher temperature (Sheng et al. 2013); (3) higher temperature would improve the complexation affinity of Eu(III) with carboxylic groups as proposed in the previous studies (Tian et al. 2010; Cai et al. 2015); (4) the increase of temperature is expected to enhance the deprotonation of carboxylic sites in the surface-linked CMC moieties (Cai et al. 2015), which would consequently improve their binding affinity toward Eu(III). The negative ΔG^0 implies the occurrence of a spontaneous process for Eu(III) binding on the Fe_3O_4@CMC composite. Specifically, the ΔG^0 values become more negative with increasing temperature, which corresponds to the improvement of sorption efficiency at higher temperature. The positive ΔS^0 value suggests the occurrence of some structural transformation and the increase of disorder after Eu(III) sorption. Overall, the sorption of Eu(III) on Fe_3O_4@CMC is a thermodynamically favorable process with an entropy increment. The temperature of the aquatic environment always fluctuates with the alteration of regions and seasons, which would affect the immobilization of heavy metal ions by solid particles. Herein, the thermodynamic data suggest that the Fe_3O_4@CMC composite can efficiently remove Eu(III) from some geological environments with elevated temperature, e.g., the geological repository.

Underlying sorption mechanisms

In order to verify the controlling mechanisms involved in the removal of Eu(III) by Fe_3O_4@CMC, desorption experiments were performed by using ammonium acetate and disodium ethylenediamine tetraacetate

Table 3 Thermodynamic parameters for Eu(III) sorption on Fe_3O_4@CMC composite

Temperature (K)	ΔH^0 (kJ/mol)	ΔS^0 (J/(mol K))	ΔG^0 (kJ/mol)
293	16.69		−18.83
313	17.59	121.25	−20.36
333	16.67		−23.68

(EDTA-2Na) as the eluents. Ammonium acetate is often employed to measure the cation exchange capacity of clays because of its favorable ion-exchange property. EDTA-2Na is usually used to elute the metal ions captured by various adsorbents because of its strong chelating property (Gao et al. 2003; Xu et al. 2016a). Specifically, the Eu(III)-adsorbed Fe_3O_4@CMC sample prepared at pH 5.5 was dispersed in the ammonium acetate solution with a concentration of 5.0×10^{-3} mol/l (100 times higher than the initial Eu(III) concentration of 5.0×10^{-5} mol/l), and the suspension was gently oscillated for 24 h. According to the ICP-AES measurement, no measurable Eu(III) was detected in the solution after the extraction experiment. This phenomenon suggests that the removal of Eu(III) is not induced by ion exchange or outer-sphere complexation. The solid phase was then gathered and soaked in the EDTA-2Na solution (5.0×10^{-3} mol/l) for an additional time period of 24 h. The ICP-AES analysis shows that the concentration of Eu(III) in supernatant is comparable to that captured by the adsorbent. In view of this, the sorption of Eu(III) on Fe_3O_4@CMC can be attributed to the inner-sphere complexation as proposed by the ignorable effect of ionic strength (Fig. 5).

The Fe_3O_4@CMC samples before and after Eu(III) sequestration were collected and characterized by using the PXRD and FTIR approaches. As shown in Fig. 8a, the PXRD pattern of the Eu(III)-loaded sample is equal to that of Fe_3O_4@CMC before sorption. The absence of new diffraction peaks rules outs the occurrence of phase transformation or the potential formation of precipitates during the sorption process. However, the FTIR spectra show some differences due to the surface binding of Eu(III) (Fig. 8b). Specifically, the band at 3418 cm^{-1} for the O–H stretching vibration shows a shift trend to lower wavelength and the absorption peak becomes broader after Eu(III) sorption. In addition, the bands at

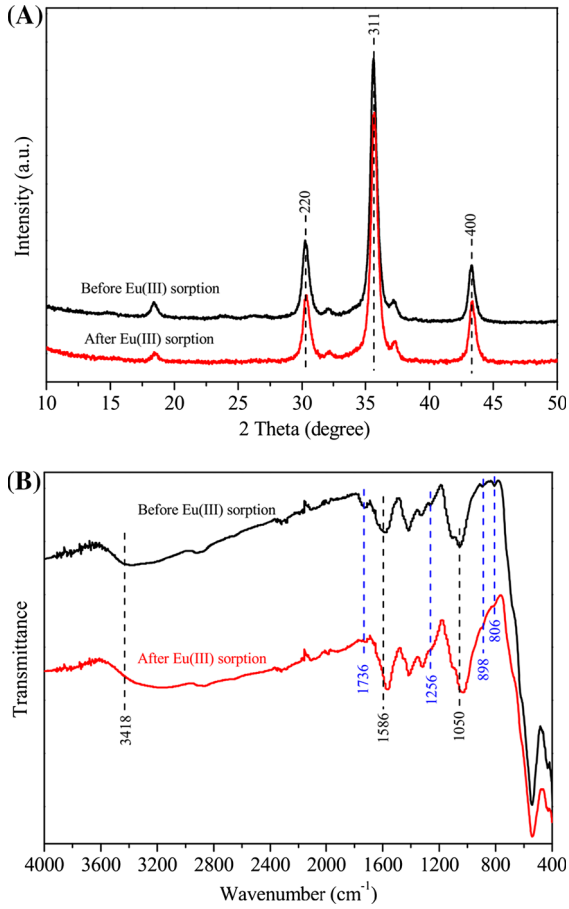

Fig. 8 PXRD patterns (**a**) and FTIR spectra (**b**) of Fe_3O_4@CMC composite before and after Eu(III) sorption

1586 cm^{-1} for the stretching vibration of the C=O bond and at 1050 cm^{-1} for the stretching vibration O–C–C bond shift to 1564 and 1029 cm^{-1}, respectively. Moreover, the relative intensity for the bands at 1736, 1256, 898 and 806 cm^{-1} is decreased with respect to that of the Fe_3O_4@CMC composite. In view of these changes and the results of desorption experiments, one can deduce that the hydroxyl (–OH) and carboxyl ($-COO^-$) sites on the surfaces of the Fe_3O_4@CMC

composite are involved in the sequestration of Eu(III), leading to the formation of inner-sphere surface complexes. The potential mechanisms mentioned herein for the capture of Eu(III) by Fe_3O_4@CMC are illustrated in Fig. 9.

Regeneration and reusability

The regeneration and reusability of the Fe_3O_4@CMC composite were explored to further evaluate its application potential in the purification of Eu(III)-polluted water systems. As mentioned above, almost 100 % of the sequestrated Eu(III) could be desorbed from the surfaces of the Fe_3O_4@CMC composite by soaking in 5.0×10^{-3} mol/l of the EDTA-2Na solution. In view of this, the same eluent was adopted herein to perform the regeneration test, and the recovered Fe_3O_4@CMC composite was then reutilized for multiple sorption/desorption experiments. As illustrated in Fig. 10, the sorption percentage of Eu(III) slightly decreases from ~80 to ~75 % after five successive cycles of sorption/desorption tests. The small decline of Eu(III) sorption percent may be due to the slight loss of Fe_3O_4@CMC dosage during the recovery process. Nevertheless, the experimental result herein shows that the synthesized Fe_3O_4@CMC composite exhibits favorable regeneration and recycling property for the removal of Eu(III). In other words, this adsorbent material can guarantee long-term application in the disposal of Eu(III)-bearing wastewater with satisfying cost performance.

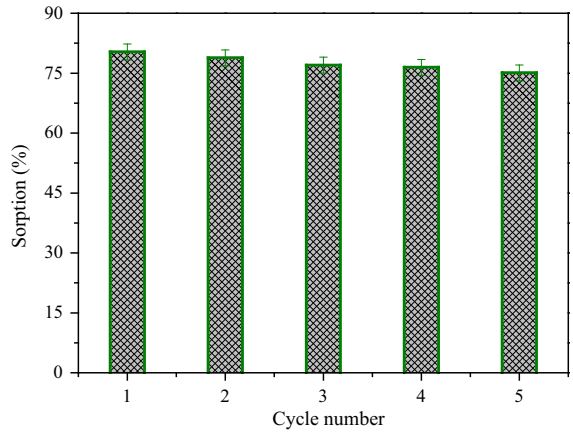

Fig. 10 Recycling of Fe_3O_4@CMC composite in the removal of Eu(III). pH = 5.5, m/V = 0.2 g/l, $C_{Eu(III)initial} = 5 \times 10^{-5}$ mol/l, $I = 0.01$ mol/l $NaNO_3$

Comparison with other adsorbents

In order to verify the superiority of applying Fe_3O_4@CMC for capturing Eu(III) from the aquatic environment, the maximum sorption capacity (q_{max}, mol/g) of

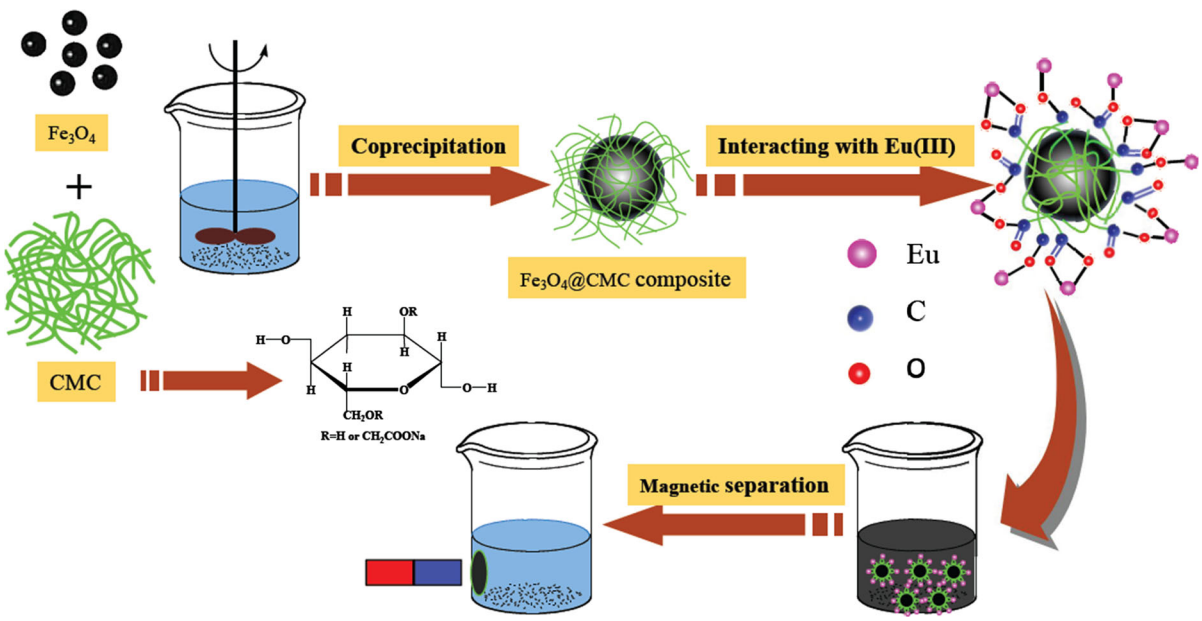

Fig. 9 Schematic illustration for the synthesis and removal mechanisms of Fe_3O_4@CMC composite toward Eu(III)

Table 4 Comparison of Eu(III) sorption capacity of Fe_3O_4@CMC with other sorbents

Materials	Experimental conditions	q_{max} (mol/g)	References
MWCNTs	pH = 4.3, T = 298 K	7.33×10^{-6}	Fan et al. (2009a, b)
TiO_2@FA	pH = 4.5, T = 293 K	1.77×10^{-5}	Tan et al. (2009)
Al_2O_3/EG	pH = 6.0, T = 293 K	3.34×10^{-5}	Sun et al. (2012)
CA membrane	pH = 5.0, T = 298 K	6.07×10^{-5}	Zaki et al. (2012)
Fe_3O_4@HA	pH = 5.0, T = 293 K	6.95×10^{-5}	Rajput et al. (2016)
PUR foam@HTTA	pH = 3.5, T = 293 K	8.20×10^{-5}	Saeed (2003)
Fe_3O_4@CD	pH = 5.0, T = 293 K	8.69×10^{-5}	Guo et al. (2015)
Fe_3O_4@CMC	pH = 5.5, T = 293 K	2.78×10^{-4}	This work
CNFs	pH = 4.5, T = 298 K	5.99×10^{-4}	Sun et al. (2016)
LDH-NaLS1	pH = 4.3, T = 293 K	1.03×10^{-3}	Mahmoud and Someda (2012)
PAO-*g*-GO	pH = 6.0, T = 303 K	1.95×10^{-3}	Sun et al. (2013)

this magnetic material toward Eu(III) was compared with those of other adsorbents as reported in the previous studies. As shown in Table 4, the q_{max} value of Eu(III) on Fe_3O_4@CMC is higher than those on multi-walled carbon nanotubes (abbreviated to MWCNTs) (Fan et al. 2009a, b), TiO_2@FA (Tan et al. 2009), expanded graphite intercalated with alumina (Al_2O_3/EG) (Sun et al. 2012), CA membrane (Zaki et al. 2012), Fe_3O_4@humic acid composite (abbreviated to Fe_3O_4@HA) (Yang et al. 2012), 2-thenoyltrifluoroacetone loaded polyurethane foam (denoted as PUR foam@HTTA) and Fe_3O_4@CD (Guo et al. 2015), while lower than those on carbon nanofibers (CNFs) (Sun et al. 2016), LDH-NaLS1 (Mahmoud and Someda 2012) and graphene oxide-supported polyaniline (PAO-*g*-GO) (Sun et al. 2013). Note that the LDH-NaLS1 material may not be stable in the acidic solution because of the potential dissolution of the LDH substrate. The potential application of CNFs and PAO-*g*-GO is also limited because of its flaws such as the complexed synthetic procedure, high synthesis cost and the ecotoxicity of carbon nanomaterials toward living beings (Akhavan and Ghaderi 2010; Yang et al. 2013b). Besides, it is inconvenient to separate these materials from the aqueous solution. The traditional centrifugation approach is unsatisfying because of the consumption of vast electric energy, which would greatly increase the cost in practical effluent disposal. Herein, the Fe_3O_4@CMC composite can be simply prepared by using the chemical co-precipitation approach with low-cost and environmental-friendly raw materials (i.e., iron salts and CMC-Na). More importantly, this material is easily collected with the aid of a magnet. Therefore, the Fe_3O_4@CMC composite would be a promising adsorbent for the remediation of Eu(III)-polluted water systems.

Conclusions

This work reported the synthesis of core–shell structured Fe_3O_4@CMC composite for the decontamination of Eu(III). The use of innoxious raw materials (iron salts and CMC-Na) and the employment of the simple co-precipitation method guaranteed the safety and cost performance of the as-prepared adsorbent. The grafted CMC improved the stability of the Fe_3O_4@CMC composite over a wide pH range. The effects of contact time, solution pH, ionic strength, solid content and temperature on the removal performance of the Fe_3O_4@CMC composite toward Eu(III) were evaluated in detail by using the batch technique. The sorption kinetics data were simulated by the pseudo-second-order model well, suggesting chemical sorption was the driving force for the sequestration of Eu(III). The sorption isotherms and corresponding thermodynamic parameters pointed to the occurrence of an endothermic and spontaneous process. Specifically, the inner-sphere surface complexation was identified to be the underlying removal mechanism. By considering the multiple advantages such as environmental friendliness, low cost, high stability, high sorption capacity, favorable regeneration performance and convenient magnetic separation property, the Fe_3O_4@CMC composite would be a potential material in the purification of polluted water containing Eu(III) and the analogous trivalent actinides (e.g., ^{241}Am and ^{244}Cm).

Acknowledgments Yawen Cai and Fang Yuan contributed equally to this paper. Financial supports from the National Natural Science Foundation of China (41203086; 21422704; 41303006), the Science Foundation of Jiangsu Province (BK20140007), "Young Thousand Talented Program" in China, the Jiangsu Provincial Key Laboratory of Radiation Medicine and Protection and the Priority Academic Program Development (PAPD) of Jiangsu Higher Education Institutions are acknowledged.

References

Akhavan O, Ghaderi E (2010) Toxicity of graphene and graphene oxide nanowalls against bacteria. ACS Nano 4:5731

Baltrusaitis J, Jensen JH, Grassian VH (2006) FTIR spectroscopy combined with isotope labeling and quantum chemical calculations to investigate adsorbed bicarbonate formation following reaction of carbon dioxide with surface hydroxyl groups on Fe_2O_3 and Al_2O_3. J Phys Chem B 110:12005

Başarır SS, Bayramgil NP (2013) The uranium recovery from aqueous solutions using amidoxime modified cellulose derivatives. IV. Recovery of uranium by amidoximated hydroxypropyl methylcellulose. Cellulose 20:827

Bulut E, Öacar M, Şengil IA (2008) Adsorption of malachite green onto bentonite: equilibrium and kinetic studies and process design. Microporous Mesoporous Mater 115:234

Cai YW, Ren XM, Lang Y, Liu ZY, Zong PF, Wang XK, Yang ST (2015) Sequestration and speciation of Eu(III) on gamma alumina: role of temperature and contact order. Environ Sci Process Impacts 17:1904

Chang YC, Chen DH (2005) Preparation and adsorption properties of monodisperse chitosan-bound Fe_3O_4 magnetic nanoparticles for removal of Cu(II) ions. J Colloid Interface Sci 283:446

Chang HX, Wu HK (2013) Graphene-based nanocomposites: preparation, functionalization, and energy and environmental applications. Energy Environ Sci 6:3483

Chen AH, Yang CY, Chen CY, Chen CY, Chen CW (2009) The chemically crosslinked metal-complexed chitosans for comparative adsorptions of Cu(II), Zn(II), Ni(II) and Pb(II) ions in aqueous medium. J Hazard Mater 163:1068

Chen H, Shao DD, Li JX, Wang XK (2014) The uptake of radionuclides from aqueous solution by poly(amidoxime) modified reduced graphene oxide. Chem Eng J 254:623

Chiou MS, Li HY (2003) Adsorption behavior of reactive dye in aqueous solution on chemical cross-linked chitosan beads. Chemosphere 50:1095

Dogsa I, Tomšič M, Orehek J, Benigar E, Jamnik A, Stopar D (2014) Amorphous supramolecular structure of carboxymethyl cellulose in aqueous solution at different pH values as determined by rheology, small angle X-ray and light scattering. Carbohydr Polym 111:492

Fan QH, Shao DD, Hu J, Chen CL, Wu WS, Wang XK (2009a) Adsorption of humic acid and Eu(III) to multi-walled carbon nanotubes: effect of pH, ionic strength and counterion effect. Radiochim Acta 97:1

Fan Q, Tan XL, Li JH, Wang XK, Wu WS, Montavon G (2009b) Sorption of Eu(III) on attapulgite studied by batch, XPS, and EXAFS techniques. Environ Sci Technol 43:5776

Fukami J, Yonemochi E, Yoshihashi Y, Terada K (2009) Evaluation of rapidly disintegrating tablets containing glycine and carboxymethylcellulose. Int J Pharm 9:101

Fukushi K, Hasegawa Y, Maeda K, Aoi Y, Tamura A, Arai S, Yamamoto Y, Aosai D, Mizuno T (2013) Sorption of Eu(III) on granite: EPMA, LA-ICP-572 MS, batch and modeling studies. Environ Sci Technol 47:12811

Gao Y, Kan AT, Tomson MB (2003) Critical evaluation of desorption phenomena of heavy metals from natural sediments. Environ Sci Technol 37:5566

Geckeis H, Lützenkirchen J, Polly R, Rabung T, Schmidt M (2013) Mineral–water interface reactions of actinides. Chem Rev 113:1016

Guo ZQ, Li Y, Pan SH, Xu JZ (2015) Fabrication of Fe_3O_4@-cyclodextrin magnetic composite for the high-efficient removal of Eu(III). J Mol Liq 206:272

Ho YS, McKay G (1999a) Pseudo-second order model for sorption processes. Process Biochem 34:451

Ho YS, McKay G (1999b) A kinetic study of dye sorption by biosorbent waste product pith. Resour Conserv Recycl 25:171

Ho YS, Ofomaja AE (2006) Pseudo-second-order model for lead ion sorption from aqueous solutions onto palm kernel fiber. J Hazard Mater B 129:137

Hokkanen S, Repo E, Suopajärvi T, Liimatainen H, Niinimaa J, Sillanpää M (2014) Adsorption of Ni(II), Cu(II) and Cd(II) from aqueous solutions by amino modified nanostructured microfibrillated cellulose. Cellulose 21:1471

Ibrahim AA, Adel AM, EI-Wahab ZHA, AIShemy MT (2011) Utilization of carboxymethyl cellulose based on bean hulls as chelating agent. Synthesis, characterization and biological activity. Carbohydr Polym 83:94

Karthik R, Meenakshi S (2015) Removal of Pb(II) and Cd(II) ions from aqueous solution using polyaniline grafted chitosan. Chem Eng J 263:168

Kaur M, Zhang HJ, Martin L, Todd T, Qiang Y (2013) Conjugates of magnetic nanoparticle actinide specific chelator for radioactive waste separation. Environ Sci Technol 47:11942

Lagoa R, Rodrigues JR (2007) Evaluation of dry protonated calcium alginate beads for biosorption applications and studies of lead uptake. Appl Biochem Biotechnol 143:115

Lamelas C, Avaltroni F, Benedetti M, Wilkinson KJ, Slaveykova VI (2005) Quantifying Pb and Cd complexation by alginates and the role of metal binding on macromolecular aggregation. Biomacromolecules 6:2756

Li Y, Sheng GD, Sheng J (2014) Magnetite decorated graphene oxide for the highly efficient immobilization of Eu(III) from aqueous solution. J Mol Liq 199:474

Lin R, Li A, Lu LB, Cao Y (2015) Preparation of bulk sodium carboxymethyl cellulose aerogels withtunable morphology. Carbohydr Polym 118:126

Liu JF, Zhao ZS, Jiang GB (2008) Coating Fe_3O_4 magnetic nanoparticles with humic acid for high efficient removal of heavy metals in water. Environ Sci Technol 42:6949

Mahmoud MR, Someda HH (2012) Mg-Al layered double hydroxide intercalated with sodium lauryl sulfate as a sorbent for $Eu^{152+154}$ from aqueous solutions. J Radioanal Nucl Chem 292:1391

Matthew B, Daniel E, Michael G, James D (2015) Carboxylated cellulose polymers for use in hydraulic fracturing operations. WIPO Patent WO/2015/123563A1 2015-08-20

Ngomsik AF, Bee A, Talbot D, Cote G (2012) Magnetic solid–liquid extraction of Eu(III), La(III), Ni(II) and Co(II) with maghemite nanoparticles. Sep Purif Technol 86:1

Obeid L, El Kolli N, Talbot D, Abramson S, Welschbillig M, Cabuil V, Bée A (2014) Adsorption of a cationic surfactant by a magsorbent based on magnetic alginate beads. J Colloid Interface Sci 432:182

Qiu L, Shao ZQ, Wang DX, Wang FJ, Wang WJ, Wang JQ (2014) Carboxymethyl cellulose lithium (CMC-Li) as a novel binder and its electrochemical performance in lithium-ion batteries. Cellulose 21:2789

Rajput S, Pittman CU, Mohan D (2016) Magnetic magnetite (Fe_3O_4) nanoparticle synthesis and applications for lead (Pb^{2+}) and chroium (Cr^{6+}) removal from water. J Colloid Interface Sci 468:334

Saeed MM (2003) Adsorption profile and thermodynamic parameters of the preconcentration of Eu(III) on 2-thenoyltrifluoroacetone loaded polyurethane (PUR) foam. J Radioanal Nucl Chem 256:73

Sankararamakrishnan N, Jaiswal M, Verma N (2014) Composite nanofloral clusters of carbon nanotubes and activated alumina: an efficient sorbent for heavy metal removal. Chem Eng J 235:1

Sheng GD, Dong HP, Shen RP, Li YM (2013) Microscopic insights into the temperature-dependent adsorption of Eu(III) onto titanate nanotubes studied by FTIR, XPS, XAFS and batch technique. Chem Eng J 217:486

Sheng GD, Yang Q, Peng F, Li H, Gao X, Huang YY (2014) Determination of colloidal pyrolusite, Eu(III) and humic substance interaction: a combined batch and EXAFS approach. Chem Eng J 245:10

Shukla A, Zhang YH, Dubey P, Margrave JL, Shukla SS (2002) The role of sawdust in the removal of unwanted materials from water. J Hazard Mater 95:137

Singh V, Ahmad S (2012) Synthesis and characterization of carboxymethyl cellulose-silver nanoparticle (AgNp)-silica hybrid for amylase immobilization. Cellulose 19:1759

Sitthichai S, Pilapong C, Thongtem T, Thongtem S (2015) CMC-coated Fe_3O_4 nanoparticles as new MRI probes for hepatocellular carcinoma. Appl Surf Sci 356:972

Sun YB, Chen CL, Tan XL, Shao DD, Li JX, Zhao GX, Yang SB, Wang Q, Wang XK (2012) Enhanced adsorption of Eu(III) on mesoporous Al_2O_3/expanded graphite composites investigated by macroscopic and microscopic techniques. Dalton Trans 41:13388

Sun YB, Shao DD, Chen CL, Yang SB, Wang XK (2013) Highly efficient enrichment of radionuclides on graphene oxide-supported polyaniline. Environ Sci Technol 47:9904

Sun YB, Wu ZY, Wang XX, Ding CC, Cheng WC, Yu SH, Wang XK (2016) Macroscopic and microscopic investigation of U(VI) and Eu(III) adsorption on carbonaceous nanofibers. Environ Sci Technol 50:4459

Tan XL, Fang M, Li JX, Lu Y, Wang XK (2009) Adsorption of Eu(III) onto TiO_2: effect of pH, concentration, ionic strength and soil fulvic acid. J Hazard Mater 168:458

Tan XL, Ren XM, Chen CL, Wang XK (2014) Analytical approaches to the speciation of lanthanides at solid–water interfaces. Trends Anal Chem 61:107

Tian GX, Martin LR, Rao LF (2010) Complexation of lactate with Neodymium(III) and Europium(III) at variable temperatures: studies by potentiometry, microcalorimetry, optical absorption, and luminescence spectroscopy. Inorg Chem 49:10598

Veliscek-Carolan J, Jolliffe KA, Hanley TL (2013) Selective sorption of actinides by titania nanoparticles covalently functionalized with simple organic ligands. ACS Appl Mater Interfaces 5:11984

Wang LY, Wang MJ (2016) Removal of heavy metal ions by poly(vinyl alcohol) and carboxymethyl cellulose composite hydrogels prepared by a freeze-thaw method. ACS Sustain Chem Eng 4:2830

Xie Y, Helvenston EM, Shuller-Nickles LC, Powell BA (2016) Surface complexation modeling of Eu(III) and U(VI) interactions with graphene oxide. Environ Sci Technol 50:1821

Xu XQ, Shen H, Xu JR, Xie MQ, Li XJ (2006) The colloidal stability and core–hell structure of magnetite nanoparticles coated with alginate. Appl Surf Sci 253:2158

Xu L, Zheng T, Yang ST, Zhang LJ, Wang JQ, Liu W, Chen LH, Diwu J, Chai ZF, Wang SA (2016a) Uptake mechanisms of Eu(III) on hydroxyapatite: a potential permeable reactive barrier backfill material for trapping trivalent minor actinides. Environ Sci Technol 50:3852

Xu SH, Zhao YG, Zheng FC, Zhang YG (2016b) Hollow Fe_3O_4@mesoporous carbon core–shell microspheres for efficient sorption of radionuclides. J Mater Sci 51:2550

Yang ST, Zhao DL, Zhang H, Lu SS, Chen L, Yu XJ (2010) Impact of environmental conditions on the sorption behavior of Pb(II) in Na-bentonite suspensions. J Hazard Mater 183:632

Yang ST, Zong PF, Ren XM, Wang Q, Wang XK (2012) Rapid and highly efficient preconcentration of Eu(III) by core–shell structured Fe_3O_4@humic acid magnetic nanoparticles. ACS Appl Mater Interfaces 4:6891

Yang K, Li YJ, Tan XF, Peng R, Liu Z (2013a) Behavior and toxicity of graphene and its functionalized derivatives in biological systems. Small 9:1492

Yang ST, Sheng GD, Montavon G, Guo ZQ, Tan XL, Grambow B, Wang XK (2013b) Investigation of Eu(III) immobilization on γ-Al_2O_3 surfaces by combining batch technique and EXAFS analyses: role of contact time and humic acid. Geochim Cosmochim Acta 121:84

Yang ST, Zong PF, Sheng GD, Ren XM, Huang YY, Wang XK (2014) New insight into Eu(III) sorption mechanism at alumina/water interface by batch technique and EXAFS analysis. Radiochim Acta 102(1–2):143

Yang ST, Ren XM, Zhao GX, Shi WQ, Montavon G, Grambow B, Wang XK (2015) Competitive sorption and selective sequence of Cu(II) and Ni(II) on montmorillonite: batch, modeling, EPR and XAS studies. Geochim Cosmochim Acta 166:129

Yeasmin MS, Mondal MIH (2015) Synthesis of highly substituted carboxymethyl cellulose depending on cellulose particle size. Int J Biol Macromol 80:725

Zaki AA, El-Zakla T, Abed El Geleel M (2012) Modeling kinetics and thermodynamics of Cs^+ and Eu^{3+} removal from waste solutions using modified cellulose acetate membranes. J Membr Sci 401–402:1

Zhang SX, Niu HY, Cai YQ, Zhao XL, Shi YL (2010) Arsenite and arsenate adsorption on coprecipitated bimetal oxide magnetic nanomaterials: $MnFe_2O_4$ and $CoFe_2O_4$. Chem Eng J 158:599

Zhivkov AM (2013) Electric properties of carboxymethyl cellulose. Chapter 8 in book Cellulose-fundamental aspects. ISBN 978-953-51-1183-2. 2013-08-28

Zhou LM, Wang YP, Liu ZR, Huang QW (2009) Characteristics of equilibrium, kinetics studies for adsorption of Hg(II), Cu(II), and Ni(II) ions by thiourea-modified magnetic chitosan microspheres. J Hazard Mater 161:995